ACSNANO

www.acsnano.org

ARTICLE

Penetrative and Sustained Drug Delivery Using Injectable Hydrogel Nanocomposites for Postsurgical Brain Tumor Treatment

Taegyu Kang,[†] Gi Doo Cha,[†] Ok Kyu Park,[†] Hye Rim Cho, Minjeong Kim, Jongha Lee, Dokyoon Kim, Bowon Lee, Jinyoung Chu, Sagang Koo, Taeghwan Hyeon,* Dae-Hyeong Kim,* and Seung Hong Choi*

Cite This: *ACS Nano* 2023, 17, 5435−5447

Read Online

ACCESS | Metrics & More | Article Recommendations | Supporting Information

ABSTRACT: **Postsurgical treatment of glioblastoma multiforme (GBM) by systemic chemotherapy and radiotherapy is often inefficient. Tumor cells infiltrating deeply into the brain parenchyma are significant obstacles to the eradication of GBM. Here, we present a potential solution to this challenge by introducing an injectable thermoresponsive hydrogel nanocomposite. As a liquid solution that contains drug-loaded micelles and water-dispersible ferrimagnetic iron oxide nanocubes (wFIONs), the hydrogel nanocomposite is injected into the resected tumor site after surgery. It promptly gelates at body temperature to serve as a soft, deep intracortical drug reservoir. The drug-loaded micelles target residual GBM cells and deliver drugs with a minimum premature release. Alternating magnetic fields accelerate diffusion through heat generation from wFIONs, enabling penetrative drug delivery. Significantly suppressed tumor growth and improved survival rates are demonstrated in an orthotopic mouse GBM model. Our system proves the potential of the hydrogel nanocomposite platform for postsurgical GBM treatment.**

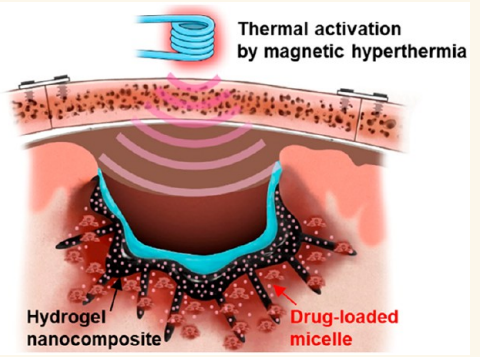

KEYWORDS: *hydrogel, nanocomposite, glioblastoma multiforme, cancer treatment, deep penetration, magnetic hyperthermia*

Patients with glioblastoma multiforme (GBM) predominantly suffer from recurrence of the disease, leading to a short average lifespan of 14.5 months even after the completion of standard treatments, including surgery, radiotherapy, and chemotherapy.[1−4] GBM cells infiltrate deeply into the brain parenchyma to obscure the border between malignant tumors and healthy brain tissues. Therefore, it is difficult to eradicate tumor cells through surgical resection without damaging healthy brain tissues, and the residual infiltrative GBM cells cause recurrence. The conventional adjuvant treatment of GBM by systemic chemotherapy and radiotherapy has shown limited efficacy due to the blood−brain barrier hindering drug penetration[5] and a decreased response to radiation because of acquired tolerance.[6] Patients whose GBM is unresectable due to the anatomical location or size of the tumor typically show even poorer prognoses and higher mortalities because they can only receive adjuvant treatments.[7]

Advanced strategies based on an understanding of the GBM microenvironment have been proposed to improve the therapeutic efficacy of systemic drug administration.[8−12] However, these methods have inherent limitations due to brain protection by the blood−brain barrier (BBB), resulting in poor therapeutic outcomes and systemic adverse effects.[13] Alternatively, local intracranial drug delivery methods have been developed to avoid these drawbacks.[14−17] This drug administration route can circumvent the BBB, deliver a high concentration of drugs directly to GBM cells while minimizing systemic toxicity, and release drugs sustainably for long-term treatment.[14,18,19] Yet, several practical challenges still remain: limited drug penetration into the perioperative region, mechanical mismatch between the implant and the brain tissues,[20] and exposure of normal brain cells and cerebrospinal fluid (CSF) to high-concentration anticancer drugs. Such unsolved issues result in insufficient efficiency of GBM therapeutics.

Recently, materials and combined therapy have been developed to improve the safety and efficacy of local

Received: October 11, 2022
Accepted: March 10, 2023
Published: March 16, 2023

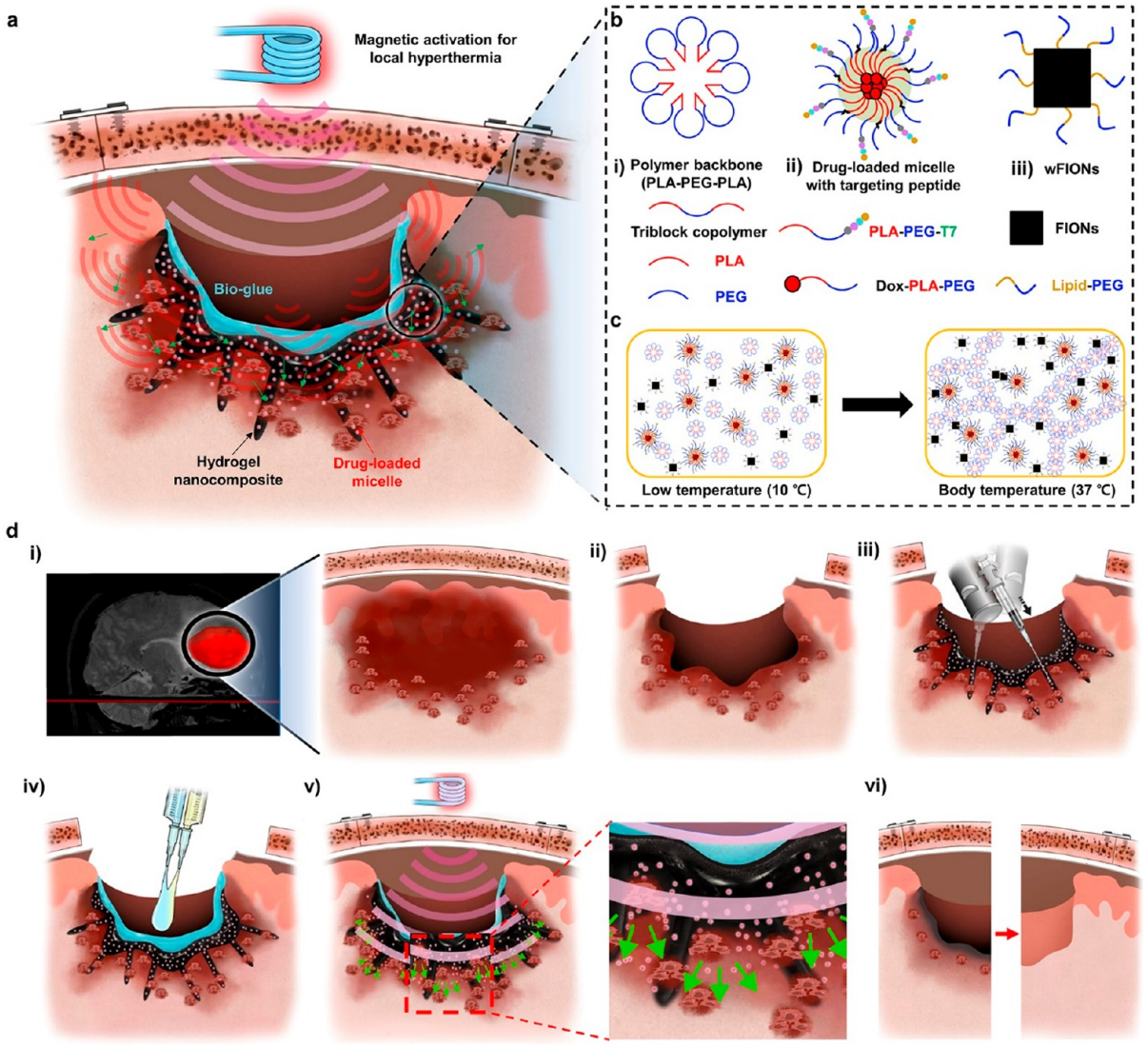

Figure 1. Penetrative drug delivery from the intracortical hydrogel nanocomposite to the deep brain tumor. (a) Schematic illustration of penetrative and sustained drug delivery to deep brain tumors from the intracortical hydrogel nanocomposite by the magnetic activation for mild hyperthermia. (b) Design of the polymer backbone, drug-loaded micelles, and water-dispersible ferrimagnetic iron oxide nanocubes (wFIONs). (c) Schematic illustration of the sol−gel transition behavior of the hydrogel nanocomposite containing the micelles and wFIONs. (d) Schematic illustrations of the GBM treatment procedure using the intracortical hydrogel nanocomposite. (i) MR-guided detection of GBM, (ii) surgical resection of GBM, (iii) injection of the hydrogel nanocomposite, (iv) coating of the bioglue, (v) periodic magnetic activation for mild hyperthermia, and (vi) biodegradation of the hydrogel nanocomposite.

intracranial drug delivery approaches. Examples include a migration-promoting hydrogel with an extracortical chemotherapeutic sink,[21] an injectable hydrogel with drug-loaded lipid nanocapsules,[22] an injectable immunostimulant hydrogel,[23] engineered hematopoietic stem cells,[24] microneedles for delivery of theranostic nanoparticles and high-energy photons,[25] engineered polymeric micromeshes,[26] and a flexible, sticky, and magnetically controlled patch.[27] Despite these research and development efforts, the complete recovery from GBM is still a daunting task. The primary challenge is how to enhance drug diffusion and penetration into the deep brain region for an extended period without severe side effects to completely kill the deeply seated residual tumor cells that can cause recurrence.

We herein present a strategy for penetrative and sustained intracortical drug delivery to eradicate residual GBM cells by using an injectable thermoresponsive hydrogel nanocomposite containing drug-loaded micelles and water-dispersible ferrimagnetic iron oxide nanocubes (wFIONs) (Figure 1a). The injection of the hydrogel nanocomposite through a syringe needle forms soft, spike-shaped intracortical drug reservoirs. This structure enables drugs to reach deeply seated residual GBM cells. The penetration of drugs can be facilitated by magnetic hyperthermia. This thermal activation of ΔT = 5 °C increases the diffusion depth of anticancer agents to reach the deeply embedded residual GBM cells. In addition, loading drugs in micelles and then into hydrogels allows for sustained drug delivery rather than rapid consumption of the drugs. Encapsulating the hydrogel nanocomposite with a bioglue minimizes leakage to CSF.

RESULTS AND DISCUSSION

Injectable Hydrogel Nanocomposite for Penetrative and Sustained Intracortical Drug Delivery. The injectable

https://doi.org/10.1021/acsnano.2c10094
ACS Nano 2023, 17, 5435−5447

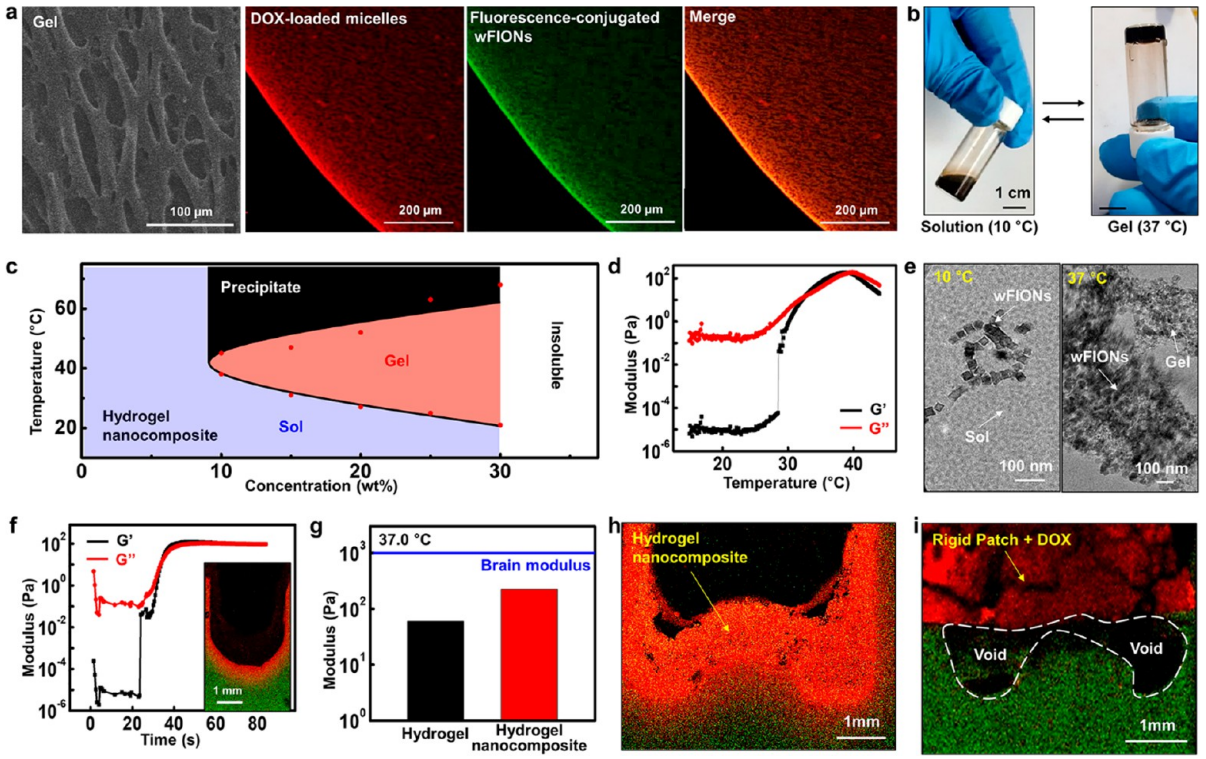

Figure 2. Design and characterization of the hydrogel nanocomposite. (a) Scanning electron microscopy image of the hydrogel nanocomposite (leftmost) and fluorescence microscopy images of the hydrogel nanocomposite containing DOX-loaded micelles and fluorescence-conjugated wFIONs (the colored frames). (b) Photographs of the hydrogel nanocomposite at different phases. (c) Phase diagram of the sol−gel transition behavior of the hydrogel nanocomposite depending on polymer concentration and temperature. Red dots indicate the experimental data. (d) Dynamic rheological analysis of the hydrogel nanocomposite depending on temperature. (G': storage modulus, G'': loss modulus). (e) Cryo-TEM images of the hydrogel nanocomposite at different temperatures. (f) Dynamic rheological analysis of the gelation time of the hydrogel nanocomposite. Inset shows a fluorescence microscopy image of the hydrogel nanocomposite (red) conformally coated on the surface of artificial brain tissue (green). (g) Moduli of the hydrogel and the hydrogel nanocomposite compared with that of the brain (blue line). (h) Fluorescence microscopy image of the hydrogel nanocomposite (red) conformally coated on the uneven surface of the artificial brain tissue (green). (i) Fluorescence microscopy image of a rigid patch containing DOX-loaded micelles (red) on the uneven surface of the artificial brain tissue (green). The black spaces between the rigid patch and the artificial brain tissue correspond to voids.

hydrogel nanocomposite consists of three components (Figure 1b): (i) thermoresponsive biodegradable polymer (poly(lactic acid-ethylene glycol-lactic acid),[28] PLA-PEG-PLA), (ii) biodegradable micelles containing structurally modified doxorubicin (DOX),[29] and (iii) wFIONs.[30] PLA-PEG-PLA is designed to gelate at body temperature (Figure 1c). The micelles consist of two types of biodegradable polymers. The backbone is PLA-PEG, either functionalized with a GBM-targeting peptide (PLA-PEG-T7)[31] or conjugated with the drug (DOX-PLA-PEG). T7 peptide can cross the BBB and selectively target GBM cells. It is anchored on the surface of DOX-loaded micelles as a targeting moiety to deliver drugs to GBM cells while minimizing damage to normal tissues.[32,33] DOX is a potent chemotherapeutic agent that has been shown to be effective in treating various malignant cancer cells, including malignant GBM cells,[34,35] but its poor penetration across the BBB limits its effectiveness in systemic GBM treatment. To address this issue, intratumoral administration of DOX was suggested, and effective therapeutic efficacy for GBM patients resistant to conventional treatments was reported.[36] With the use of the hydrogel nanocomposite system, local delivery of the DOX-loaded micelles can be achieved, making DOX a potential candidate for GBM treatment. wFIONs generate heat locally through hyperthermia under an external magnetic field, accelerating the diffusion of micelles and drugs.[37,38]

The schematic of the administration method is shown in Figure 1d: (i) the morphology and volume of GBM are detected by magnetic resonance (MR) scanning; (ii) the bulk tumor is removed by surgical resection; (iii) the hydrogel nanocomposite solution is injected into multiple locations of the postoperative brain cavity up to the parenchyma surface and gelated to form intracortical drug reservoirs; (iv) a degradable bioglue (EVICEL, Ethicon, USA) is applied on the hydrogel nanocomposite, and the cranium is restored; (v) the alternating magnetic fields (AMFs)-induced mild hyperthermia prompts the diffusion of micelles and drugs from hydrogel nanocomposite into the postoperative margin in the deep brain region (magnified view). The thermal activation by AMFs is repeated every other day for 2 weeks; (vi) the remaining drug payload is released *via* spontaneous diffusion, and the hydrogel nanocomposite is degraded.

The proposed materials and method are promising candidates for the postsurgical treatment of GBM due to the following advantages: (i) anticancer drugs are locally delivered to the GBM site, bypassing the BBB; (ii) spike-shaped intracortical drug reservoirs and AMF-activated hyperthermia help drugs reach deeply infiltrative GBM cells; (iii) soft

https://doi.org/10.1021/acsnano.2c10094
ACS Nano 2023, 17, 5435−5447

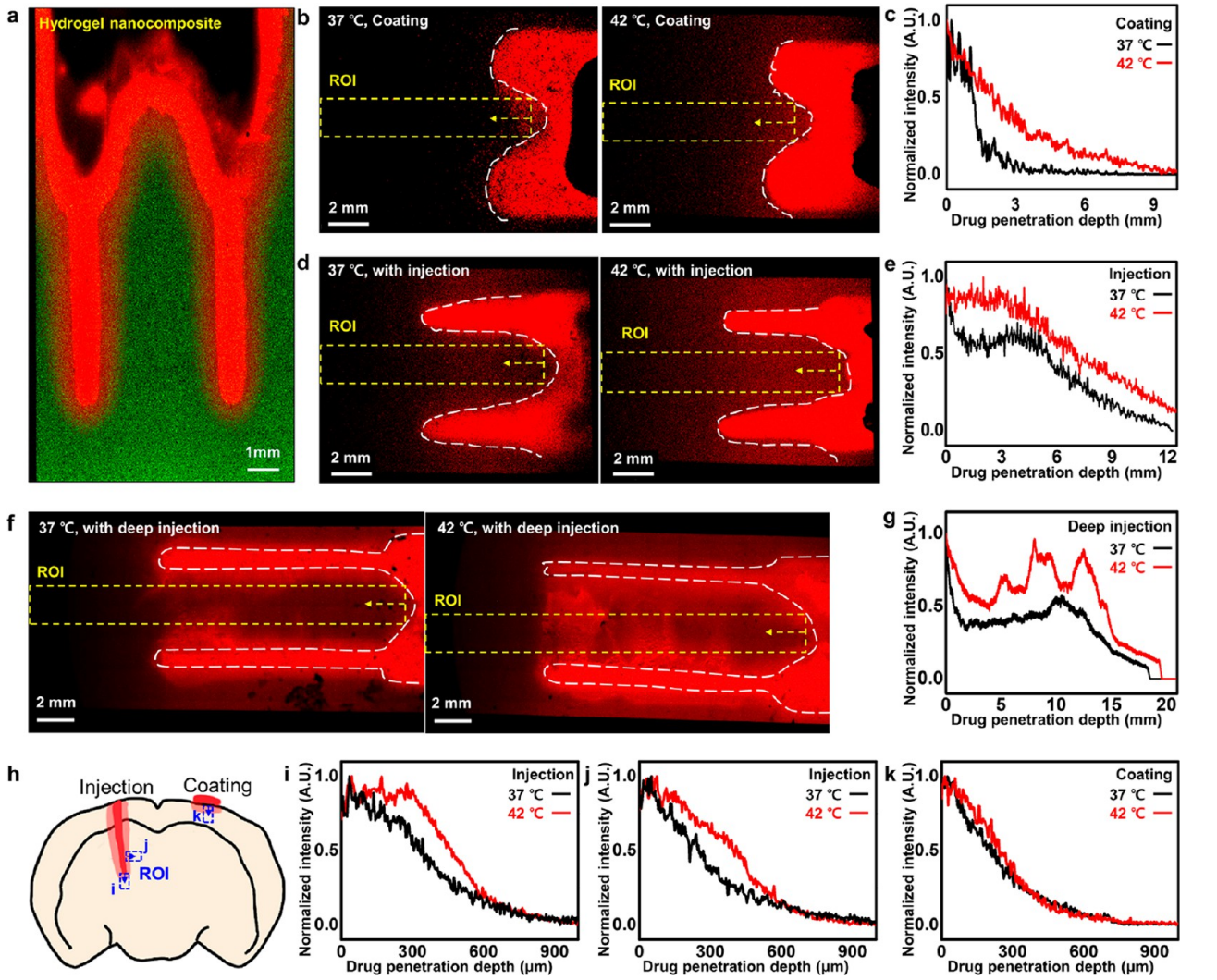

Figure 3. Deep penetration of the drug. (a) Fluorescence microscopy image of the hydrogel nanocomposite (red) injected into the artificial brain tissue (green). (b) Fluorescence microscopy images that show the distribution of the DOX molecules diffused from the hydrogel nanocomposite (red) to the artificial brain tissue (black) at 37 °C (left) and 42 °C (right) after 3 h and (c) the normalized fluorescence intensity of the regions of interest (ROIs). (d) Fluorescence microscopy images that show the distribution of the DOX molecules diffused from the syringe-injected hydrogel nanocomposite (red) to the artificial brain tissue (black) at 37 °C (left) and 42 °C (right) after 3 h and (e) the normalized fluorescence intensity of the regions of interest (ROIs). (f) Fluorescence microscopy images that show the distribution of the DOX molecules diffused from the deeply syringe-injected hydrogel nanocomposite (red) to the artificial brain tissue (black) at 37 °C (left) and 42 °C (right). (g) Normalized fluorescence intensities in the ROIs at 37 and 42 °C. The ROIs are drawn in (f). (h) Schematic illustration of the administration method of the hydrogel nanocomposite to the mouse brain *in vivo*. (i) Normalized fluorescence intensities for the ROI to the longitudinal direction from the bottom of the injected hydrogel nanocomposite. The ROIs are drawn in (h). (j) Normalized fluorescence intensities for the ROI to the transversal direction from the side of the injected hydrogel nanocomposite. The ROIs are drawn in (h). (k) Normalized fluorescence intensities for the ROI to the longitudinal direction from the bottom of the coated hydrogel nanocomposite. The ROIs are drawn in (h).

mechanical properties of the hydrogel nanocomposite minimize mechanical mismatch between the brain tissues and the implant; (iv) fluid injection of the nanocomposite solution ensures the establishment of a conformal interface between the nanocomposite and the brain, and additional coverage with bioglue minimizes unwanted drug leakage to CSF; (v) drugs are contained in micelles for sustained release; (vi) cocktail of anticancer agents can be incorporated into the nanocomposite to address the heterogeneity of GBM; and (vii) biodegradation and biocompatibility of the hydrogel nanocomposite minimize the foreign body responses and obviate follow-up surgery for its retrieval.

Material Design and Characterization of the Injectable, Thermoresponsive Hydrogel Nanocomposite. The confocal laser scanning microscopy (CLSM) images confirm the homogeneous dispersion of micelles and fluorescein-conjugated wFIONs inside the hydrogel nanocomposite (Figure 2a). The hydrogel matrix consists of a triblock copolymer, PLA-PEG-PLA. The molecular weight of each polymer block is designed as 1380−1450−1380 for facile gelation at the desired temperature (Figure S1a). The sol−gel transition behavior depends on the polymer concentration and temperature (Figure S1b, c).

The hydrogel nanocomposite is in a solution phase at 10 °C. However, it transforms into a gel at body temperature (37 °C;

https://doi.org/10.1021/acsnano.2c10094
ACS Nano 2023, 17, 5435−5447

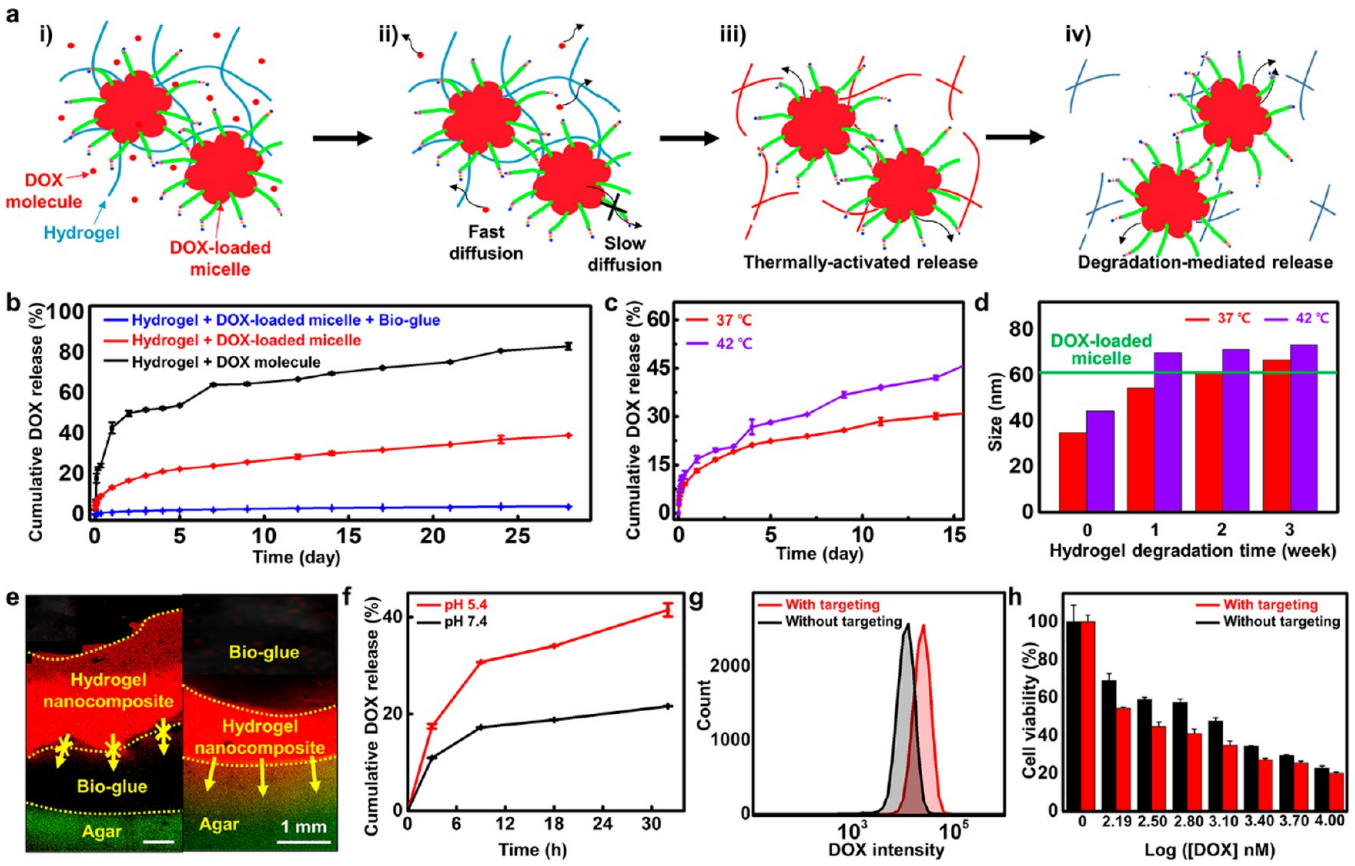

Figure 4. DOX-loaded micelle for sustained, targeted, and controlled drug delivery. (a) Schematic illustrations that portray the time- and temperature-dependent drug release from the hydrogel nanocomposite and the corresponding mesh sizes of the hydrogel matrix: (i) initial state, (ii) release of DOX molecules, (iii) release of DOX molecules and DOX-loaded micelles by thermal activation, and (iv) release of DOX molecules and DOX-loaded micelles upon degradation of the hydrogel. (b) Profile of time-dependent DOX release from the hydrogel nanocomposite (black: hydrogel with DOX molecules, red: hydrogel with DOX-loaded micelles, blue: hydrogel with DOX-loaded micelles and covered with the bioglue). (data: mean ± s.d., n = 3). (c) Time profile of DOX-loaded micelle release from the hydrogel nanocomposite at 37 °C (red) and 42 °C (purple). (data: mean ± s.d., n = 3). (d) Temporal changes in mesh size of the hydrogel matrix at 37 °C (red) and 42 °C (purple). The hydrodynamic size of the DOX-loaded micelles is indicated as a green line. (e) Fluorescence microscopy images of the DOX molecules diffused from the hydrogel nanocomposite to the artificial brain tissue with (left) and without (right) a bioglue layer between the nanocomposite and the artificial tissue. (f) pH-dependent drug release from the DOX-loaded micelles. (data: mean ± s.d., n = 3). (g) Representative flow cytometry histograms of U-87 MG cells incubated with the DOX-loaded micelles with (red) or without (black) the targeting moiety. (h) MTT cell viability test results of the GBM cells treated with various concentrations of the DOX-loaded micelles with (red) or without (black) the targeting moiety. (data: mean ± s.d., n = 3).

Figure 2b,c), similar to the gelation behavior of a bare hydrogel (Figure S1b,c). According to dynamic rheological analysis, the sol−gel transition temperature, at which the storage modulus (G') becomes larger than the loss modulus (G''), is ∼32 °C (Figure 2d). Gelation entails structural changes. Observations from cryogenic-transmission electron microscopy (Cryo-TEM) images reveal that micelles and wFIONs are dispersed in the solution-state hydrogel but aggregated in the gel state (Figure 2e). Incorporating the micelles and wFIONs into the hydrogel rarely affects its inherent sol−gel transition properties (Figure 2d,e, Figure S1d,e).

The physical properties of the hydrogel nanocomposite are optimized in consideration of the intracortical environment. The time for the sol−gel transition is ∼40 s, as estimated by the rheological analysis (Figure 2f). This fast gelation enables seamless coating of the sidewall of the brain parenchyma with the hydrogel nanocomposite. The fluorescence imaging also shows that the nanocomposite solution injected into the artificial brain parenchyma gelates immediately and forms a conformal interface (Figure 2f, inset). The hydrogel nanocomposite has a lower modulus than the brain tissue, which can minimize mechanical mismatch (Figure 2g).[39]

Due to the rapid gelation and soft physical properties of the hydrogel nanocomposite, the rugged surface of the artificial brain tissue can be seamlessly covered by the nanocomposite (Figure 2h). On the contrary, a rigid implant cannot form such a conformal interface with the convoluted brain surface (Figure 2i). The voids between the rigid device and the brain surface can be filled with the CSF, which induces premature drug leakage from the implant to the CSF, decreasing the drug delivery efficiency to the brain tumor and causing side effects.

Deep Penetration and Extended Diffusion of the Loaded Drug. The hydrogel nanocomposite can be injected into the perioperative margin of the brain *via* a syringe, forming soft drug reservoirs in the target region. The implantation depth of the hydrogel nanocomposite into the brain and the spacing between injection sites can be manually controlled during the injection process (Figure 3a). This property represents a significant advantage to using the

https://doi.org/10.1021/acsnano.2c10094
ACS Nano 2023, 17, 5435−5447

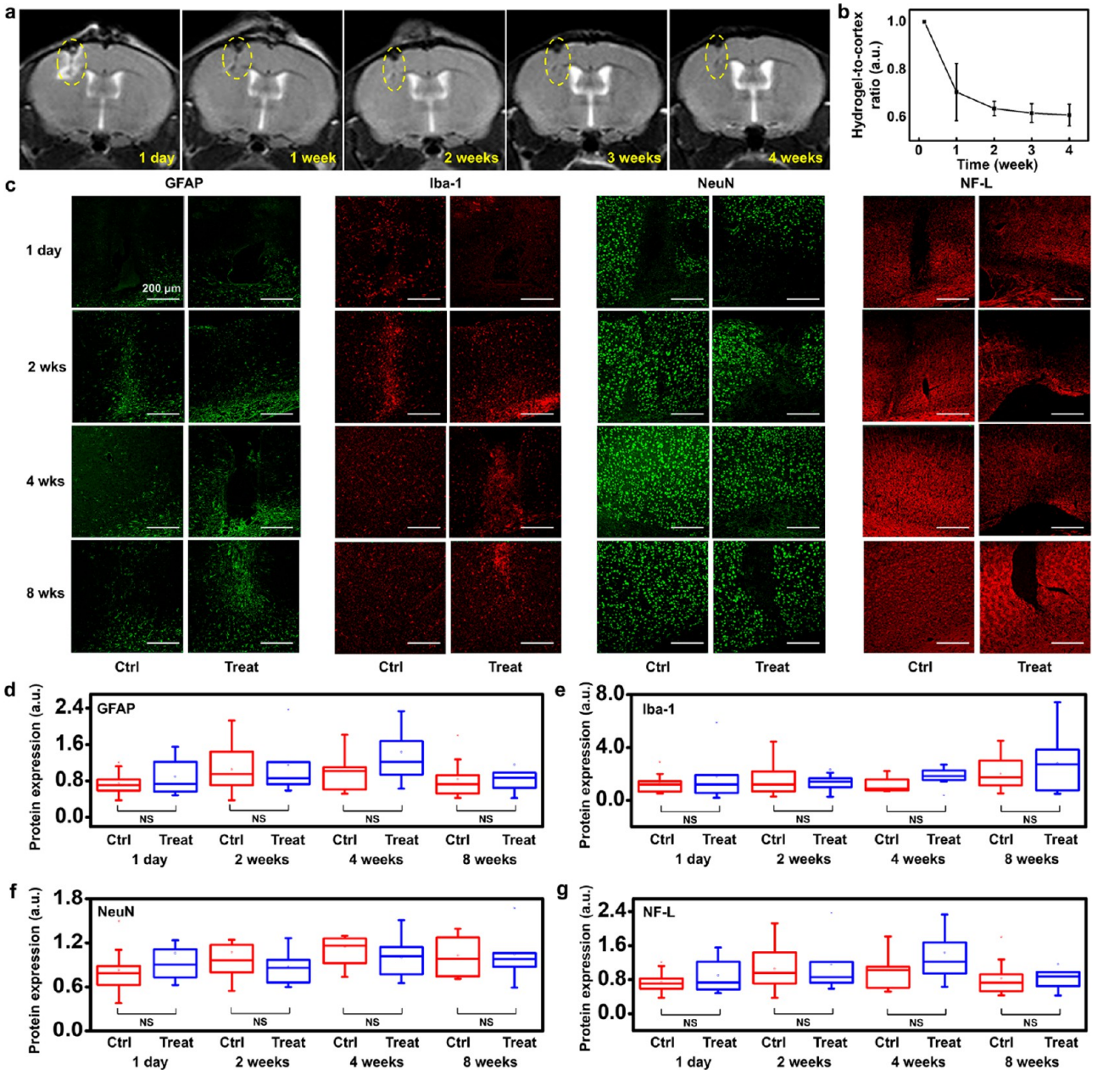

Figure 5. Biodegradability of the hydrogel nanocomposite. (a) MR images of the mouse brain injected with the hydrogel nanocomposite obtained at various postinjection time points (1 day, 1 week, 2 weeks, 3 weeks, and 4 weeks after injection). The yellow dotted circles indicate the hydrogel nanocomposite. (b) Time-dependent change in the MR signal intensity ratio of the hydrogel nanocomposite to the cortex area. (data: mean ± s.d., n = 6). (c) Fluorescence microscopy images of the brain tissues at the injection sites of the control (Ctrl, left) and the treatment (Treat, right) groups at various postinjection time points (1 day, 2, 4, and 8 weeks). The tissues were labeled by GFAP (green, left), Iba-1 (red, left), NeuN (green, right), and NF-L (red, right). (d–g) Quantification of Western blot analysis of the immune-related proteins ((d) GFAP; (e) Iba-1; (f) NeuN; (g) NF-L) at different time points for the control (red) and the treatment (blue) groups. Line: median, box: 25th to 75th percentiles, whisker: min to max (n = 9 for each group). (NS; p > 0.05 by Mann–Whitney U-test).

hydrogel nanocomposite in the postsurgical treatment of deeply infiltrated GBM cells.

Additionally, hyperthermia induced by wFIONs under AMFs promotes the immediate release and the extended diffusion of the drug. This hyperthermic effect is maximized when wFIONs with a core size of 22 nm (Figure S2a,b) are well dispersed at a concentration of 100 mM. wFIONs exhibit a high saturation magnetization[30] and negligible leakage from the hydrogel (<1% after 2 weeks; Figure S2c). The temperature is increased by a maximum of ∼5 °C (*i.e.*, mild hyperthermia) to prevent thermal damage to the normal brain tissues. For hydrogel nanocomposite solutions of 50 and 150 μL, each containing 100 mM wFIONs, optimal distances from the external coil are 9 and 12 mm, respectively (Figure S2d–i).

We measured the fluorescence intensity of released DOX molecules in artificial brain tissues to observe enhanced drug penetration. DOX was diffused either from the nanocomposite coated on the artificial tissue surface or from the nanocomposite injected into the artificial tissue, and the fluorescence after 3 h was compared at 37 °C (left) and 42 °C (right). The drug diffused from the nanocomposite on the artificial tissue surface shows a limited penetration, although

https://doi.org/10.1021/acsnano.2c10094
ACS Nano 2023, 17, 5435–5447

the thermal activation improves the penetration to a certain extent (Figure 3b,c). In contrast, the nanocomposite injected into the artificial tissue allows for a much deeper penetration of DOX (Figure 3d,e). In particular, due to the thermally enhanced diffusion, DOX can also fill the region between two injected hydrogel nanocomposites.

Considering potential clinical translation, the centimeter-scale penetration of drugs is advantageous to treating deeply located GBM cells. When the nanocomposite is injected deeply (~12 mm) into the artificial brain tissue, thermal activation drives the drugs to diffuse up to ~15 mm, as shown by the quantitative measurement of the DOX diffusion (Figure 3f,g). These results support the idea that the deep syringe injection combined with magnetic hyperthermia can achieve highly penetrative drug delivery.

We quantified the DOX diffusion in the mouse brain *in vivo* (Figure 3h). In the syringe-injected hydrogel nanocomposite group with thermal activation, the drug can be delivered deeply in both transversal and longitudinal directions (Figure 3i,j). However, in the coating group, the penetration of DOX is shallow, even with thermal activation (Figure 3k). The syringe injection of the hydrogel nanocomposite not only allows deep penetration of the drug but also increases the contact area between the nanocomposite and the tissue, which can facilitate drug delivery. Mild hyperthermia can also increase drug diffusion by enhancing perfusion and vascular permeability *in vivo*.[40] As a result, the tailored administration method of the hydrogel nanocomposite, syringe injection combined with thermal activation, can potentially increase the therapeutic efficacy for GBM.

Drug-Loaded Micelles for Sustained, Targeted, and Controlled Drug Delivery. The DOX-loaded micelles are synthesized by using a nanoprecipitation method (Figure S3a). The DOX-loaded micelle is composed of two types of amphiphilic diblock copolymers, one with a maleimide moiety to conjugate a peptide for targeting GBM (PLA-PEG-maleimide) and the other with an acid-cleavable linkage for pH-responsive release of DOX (NH_2-NH-PLA-PEG) for sustained, targeted, and controlled drug delivery. A GBM-targeting peptide (T7) is linked to the maleimide group. The synthesis of each polymeric component is confirmed by ^{1}H NMR (Figure S3b,c). The hydrodynamic diameter of the DOX-loaded micelles, measured by dynamic light scattering, is 61 nm (Figure S3d). The drug encapsulation efficiency and loading capacity, determined by a fluorescence spectrometer, were 52.8% and 2.4%, respectively. The grafting efficiency of T7 peptide is 53.7%.

The synthetic protocol can also accommodate other drugs, such as temozolomide (TMZ) (Figure S4a,b). TMZ-loaded micelles show cytotoxicity to U-87 MG cells, and the hydrogel nanocomposite containing TMZ-loaded micelles exhibits sol–gel transition behavior to that of its DOX counterpart (Figure S4c,d). Furthermore, we confirm that different types of drug-loaded micelles can be loaded in a hydrogel nanocomposite with a predefined ratio, showing the capability of delivering multiple therapeutics for rationally designed combination therapy (Figure S4e–i).

The drug release depends on the hydrodynamic sizes of the payload (drugs and micelles) relative to the mesh size of the hydrogel matrix (Figure 4a).[41] DOX molecules trapped in the hydrogel nanocomposite can diffuse out rather easily. Nonetheless, the spontaneous release of DOX-loaded micelles is suppressed because their hydrodynamic size is larger than that of the DOX molecules. The time-dependent biodegradation of the hydrogel induces a gradual increase in the mesh size of the hydrogel, facilitating the release of trapped micelles. Thermal activation can cause temperature-dependent swelling of the hydrogel matrix, promoting the release of both DOX molecules and DOX-loaded micelles.

We monitored the drug release profile *in vitro*. Drug release from DOX-loaded micelles (Figure 4b, red) is suppressed compared to the release of DOX molecules without micelles (Figure 4b, black). A modest increase in drug release over time is observed as the hydrogel degrades. An increased drug release under heating (ΔT = 5 °C) *in vitro* is also confirmed (Figure 4c). These time-dependent and thermally driven release profiles correspond well with the change in hydrogel mesh size, which increases at higher temperatures and with longer biodegradation periods (Figure 4d). Moreover, the effective blocking of drug diffusion from the nanocomposite by the bioglue was confirmed by fluorescence imaging (Figure 4e). The prevention of unwanted drug leakage to the CSF by the coating of the bioglue on the hydrogel nanocomposite was also demonstrated *in vitro* (Figure 4b, blue).

The pH-responsive linkage (hydrazone bond) between DOX and the terminal end of PLA-PEG is cleaved under acidic conditions near tumor tissues or within the endosomes of GBM cells. Therefore, the DOX release is expedited at acidic pH (5.4; tumor endosomal pH) compared to physiological pH (7.4; Figure 4f). Furthermore, the targeting peptide anchored on micelles effectively binds to the transferrin receptors, which are upregulated on the surface of GBM cells, leading to higher uptake of DOX-loaded micelles by U-87 MG cells than those without the targeting moiety (Figure 4g and Figure S5). As a result, the cytotoxicity of DOX-loaded micelles can be enhanced (Figure 4h).

Biodegradability of the Hydrogel Nanocomposite. To test the biodegradability of the hydrogel nanocomposite *in vivo*, a hydrogel nanocomposite without drugs was injected into the mouse brain. Its degradation was monitored by T2-weighted MR imaging at various time points (Figure 5a). At first, the hydrogel nanocomposite (Figure 5a left, yellow circle) appears as black, which is not observed in the control group (Figure S6a), and degrades as time elapses (the rest frames of Figure 5a). For quantitative analysis, the ratios of the MR signal intensities between the hydrogel nanocomposite and the normal brain tissue were obtained at various time points (Figure 5b and Figure S6b). The gradual decrease in the ratio can be correlated with a gradual degradation of the hydrogel nanocomposite (~60% at 4 weeks after the implantation). MR images also show that injection of the hydrogel nanocomposite does not cause side effects, such as intracerebral swelling.[42] Additionally, the biodegradation profile of the hydrogel nanocomposite was monitored after intramuscular and subcutaneous injections (Figure S7). The hydrogel nanocomposite was mostly degraded after 2 weeks and entirely disappeared after 4 weeks. The stability of the hydrogel nanocomposite (Figure S8) was observed *in vitro* by soaking it in a phosphate-buffered saline (PBS) solution, which is consistent with the results of *in vivo* biodegradability experiments.

The biocompatibility of the hydrogel nanocomposite in brain tissue was evaluated by immunohistochemical staining at various time points (Figure 5c).[43] The hydrogel nanocomposite without drugs was injected into mice brains, and astrocytes (glial fibrillary acidic protein (GFAP), green),

https://doi.org/10.1021/acsnano.2c10094
ACS Nano 2023, 17, 5435–5447

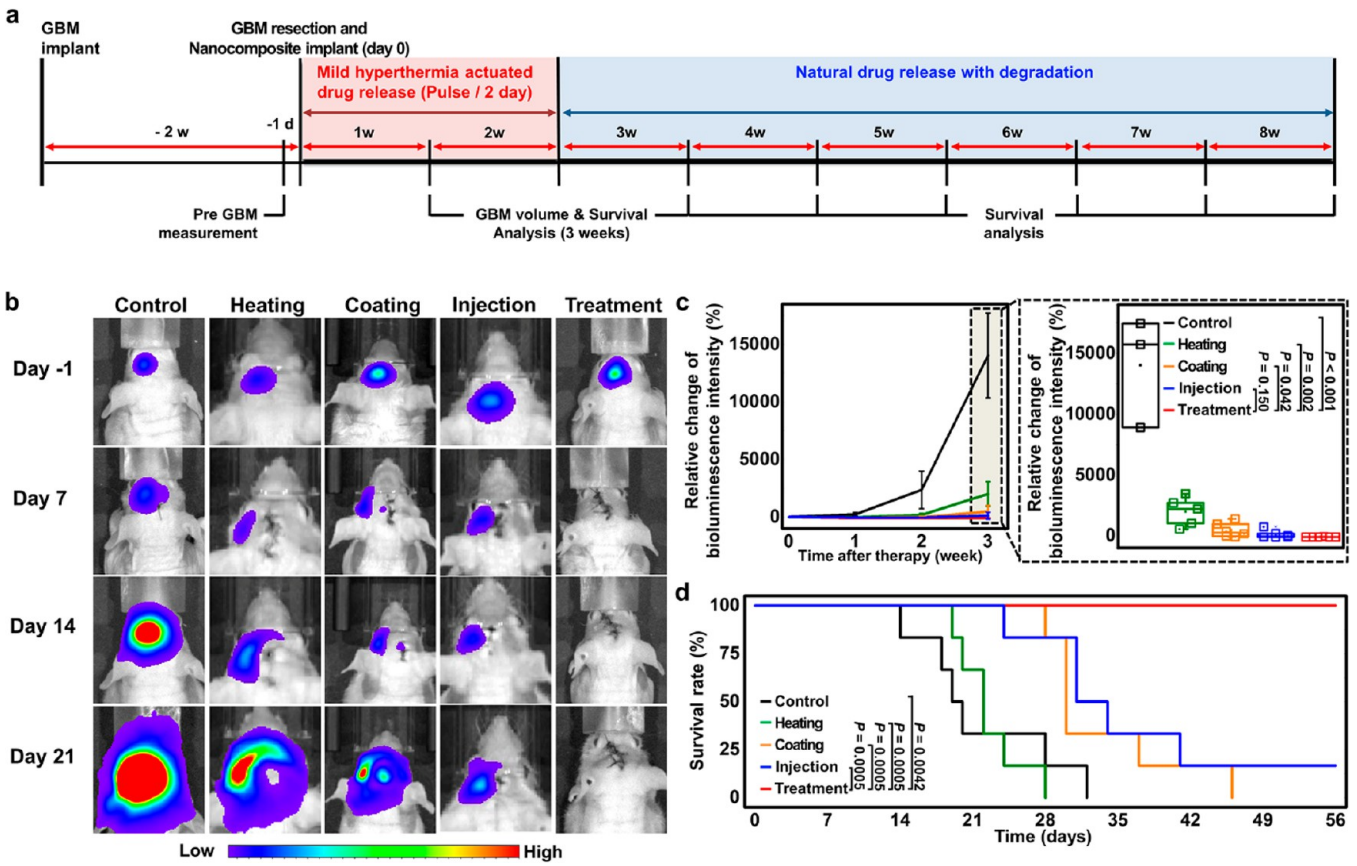

Figure 6. Postsurgical treatment efficacy of the hydrogel nanocomposite in the mouse brain GBM model. (a) Schematic illustration that shows the treatment schedule. (b) *In vivo* luminescence imaging results of GBM volumes for the control, heating, coating, injection, and treatment groups at indicated time points (1 day before, 1 week, 2 weeks, and 3 weeks after the treatment). (c) Time-dependent relative change of bioluminescence intensity for the control (black), heating (green), coating (orange), injection (blue), and treatment (red) groups at indicated time points (left; $n = 6$ for each group; Data are presented as means ± s.d.) and comparison among the relative change of bioluminescence intensity 3 weeks after the treatment (right), Line: median, box: 25−75th percentiles, whisker: min to max ($n = 3$ for control, $n = 5$ for heating, and $n = 6$ for coating, injection, and treatment groups; statistical comparisons were tested by one-way analysis of variance (ANOVA) with Scheffe multiple comparison tests). (d) Kaplan−Meier survival rates for the control (black), heating (green), coating (orange), injection (blue), and treatment (red) groups ($n = 6$ for each group; statistical comparisons were tested by log-rank test).

microglia (ionized calcium-binding adapter molecule (Iba-1), red), neuron somata (neuronal nuclear antigen (NeuN), green), and axons (neurofilament light polypeptide (NF-L), red) in brain tissues were stained with antigen-specific fluorescent dyes. In the control group, PBS was injected with the same administration protocol instead of the hydrogel nanocomposite. The treatment group did not show a significant increase in the expression of microglia, accumulation of astrocytes, and depletion of neurons (Figure 5c, right columns) around the implanted site, compared with the control group (Figure 5c, left columns) over the entire 8-week period. The expressions of these immunogenic markers were quantified by using Western blot analysis (Figure S9). No significant difference was observed between the treated and control groups in the quantitative analysis (Figure 5d−g). These results imply that the hydrogel nanocomposite does not induce severe short-term or long-term immune responses and neuronal damage and support the biocompatibility of the hydrogel nanocomposite in the intracerebral microenvironment. Moreover, it is noteworthy that these findings could also address potential concerns about brain damage by using the syringe-injection method.

Verification of Therapeutic Efficacy *In Vivo*. We prepared an orthotopic mouse GBM resection model to evaluate the therapeutic efficacy of the proposed materials and method *in vivo*. We implanted luciferase-expressing GBM cells (U-87 MG-Luc2, ATCC) into the cerebral cortex of each mouse. The appropriate time for surgical removal of the GBM was approximately 2 weeks after the implantation, which was determined by monitoring MR imaging and *in vivo* imaging system (IVIS) measurement to establish the GBM resection model (Figure S10a,b). The change in bioluminescence signal before and after the resection surgery was detected (Figure S10c,d) to confirm the effectiveness of the resection surgery. Then, the mice were divided into five groups to evaluate whether the treatment efficacy for GBM treatment could be improved by deep penetration of the drug: (i) control group: tumor resection and PBS injection, (ii) heating group: tumor resection, injection of the hydrogel nanocomposite without any chemotherapeutic drugs, and hyperthermia treatment, (iii) coating group: tumor resection, coating of the hydrogel nanocomposite with drugs, and no hyperthermia treatment, (iv) injection group: tumor resection, injection of the hydrogel nanocomposite, and no hyperthermia treatment; (v) treatment group: tumor resection, injection of the hydrogel nanocomposite, and hyperthermia treatment.

For the injection and treatment group, the hydrogel nanocomposite containing drugs was injected into multiple

https://doi.org/10.1021/acsnano.2c10094
ACS Nano 2023, 17, 5435−5447

sites of the tumor resection region and then coated on the brain surface. For the heating group, the same procedure as that for the treatment group was employed, but the nanocomposite without any chemotherapeutic drugs was used. For the coating group, the hydrogel nanocomposite with drugs was coated on the tumor resection region without injection. For all groups, a bioglue was applied on the top surface, and then the skin was repositioned and sutured. The heating and treatment groups received hyperthermia for 30 min every other day during the first 2 weeks, and the natural release of the remaining drugs followed (Figure 6a). Detailed conditions and methods for *in vivo* experiments are described in the Methods.

Treatment efficacy was assessed by monitoring the bioluminescence signal from tumor tissue using IVIS and quantifying the signal change in the region of interest (Figure 6b). As presented in Figure 6c, the treatment group shows a tumoricidal effect over 3 weeks compared with other groups. The treatment group showed steady tumor regression, while other groups showed rebounding or delayed tumor growth during the 3 weeks. The mean tumor volume change for 3 weeks in the control, heating, coating, and injection groups are +14,031%, +1,993%, +469%, and +111%, respectively, while that of the treatment group is −94.13% (Figure 6c, right; $p < 0.001$ compared to control group, $p = 0.002$ compared to heating group, $p = 0.042$ compared to coating group, and $p = 0.150$ compared to injection group). The comparison between coating and injection groups showed that the GBM growth could be suppressed more significantly by the syringe-injection method of the hydrogel nanocomposite. Besides, the comparison between injection and treatment groups highlights the importance of achieving a potential tumoricidal effect in the initial period with the assistance of mild hyperthermia. The injection group showed some (but insufficient) tumor removal effect in the initial 3 weeks, compared to that of the treatment group, and eventually, the tumor in the injection group was regrown in 4 weeks (Figure S11; $p = 0.0087$).

This significant suppression of the tumor volume in the treatment group leads to a much higher survival rate compared to all other control groups, with all mice surviving at least 8 weeks (Figure 6d; $p = 0.0005$ compared to control, heating, and coating groups, and $p = 0.0042$ compared to injection group). The injection group shows extended median survival of 32.5 days, with one mouse surviving for 8 weeks, while no mice in other control groups survived more than 46 days (median survival of 19.5, 22, and 30 days for control, heating, and coating groups, respectively). The results of the hematoxylin and eosin (H&E) staining and terminal deoxynucleotidyl transferase dUTP nick end labeling (TUNEL) assay also confirm that the treatment group underwent an effective treatment effect (Figure S12). These results support the idea that the injectable hydrogel nanocomposite associated with the optimized protocol shows nearly complete inhibition of GBM recurrence after resection in a preclinical model.

CONCLUSIONS

The therapeutic efficacy of conventional GBM treatment methods has been insufficient due to the high invasiveness of GBM. In particular, deeply infiltrative GBM cells that cannot be surgically removed cause the recurrence of GBM. To tackle this issue, we developed an injectable hydrogel nanocomposite and its *in vivo* application protocol optimized for the postsurgical treatment of deeply infiltrative GBM cells. A hydrogel nanocomposite solution that contains drug-loaded micelles and wFIONs is injected into the brain parenchyma at multiple locations to form soft intracortical drug reservoirs. Under AMFs, wFIONs generate heat to expedite the release and diffusion of the micelles and the drugs, enabling centimeter-deep drug penetration. The micelles are designed to suppress premature drug release, target GBM cells, and release the drug payload in response to the acidic tumor microenvironment. We also established an application protocol for using the nanocomposite with the orthotopic mouse GBM model *in vivo*. Tumor growth can be notably suppressed, and the survival rate can be markedly improved. Given the proven biocompatibility and high therapeutic efficacy in the preclinical GBM model, the proposed materials and protocol are expected to serve as a promising solution for effective postsurgical treatment. Moreover, this method is potentially applicable to patients with unresectable GBM and can synergize the effects of conventional therapeutic approaches or multimodal solutions.[44] Further studies concerning the physiological complexity of GBM,[45] such as immune reactions, tumor size effect, and tumor microenvironments, would be required to advance the proposed system toward clinical translation.

EXPERIMENTAL SECTION

Methods. *Synthesis of the Backbone Polymer of the Thermoresponsive Hydrogel.* The triblock PLA-PEG-PLA copolymer of block molecular weights 1380−1450−1380 was synthesized by ring-opening copolymerization of D,L-lactide (Thermo Fisher, USA) with PEG (Merck KGaA, Germany) using stannous octoate (Thermo Fisher, USA) as a catalyst.[46] PEG (10.00 g, 6.67 mmol) was heated to 100 °C and vacuum-dried for 2 h to remove the remaining water. After cooling, D,L-lactide (19.00 g, 131.95 mmol) was added, and the mixture was heated to 100 °C for dissolution. A catalytic amount of stannous octoate was added, and the reaction was carried out at 140 °C for 10 h under Ar atmosphere. After the reaction, the flask was cooled in an ice bath. The resulting PLA-PEG-PLA block copolymer was dissolved in chloroform, and an excess amount of precooled hexane was added to precipitate the polymer. The supernatant was decanted, and the sediment was dried in a vacuum oven at 50 °C to remove the residual solvent. The chemical structure of the hydrogel precursors was analyzed using a ^{1}H NMR spectrometer (Avance III 500, Bruker, Germany) at the National Center for Inter-University Research Facilities (NCIRF) of Seoul National University.

Preparation of the Hydrogel Nanocomposite. The backbone polymer was dissolved in various concentrations in a PBS solution (Thermo Fisher, USA). These solutions were stirred in a refrigerated environment (4 °C) until a homogeneous transparent state was acquired. The successful preparation of the polymer solution was confirmed by its thermoresponsive gelation at 37 °C. After preparing the polymer solution, the drug-loaded micelles and wFIONs were added to the polymer solution to obtain a nanocomposite solution. The drug-loaded micelles were dissolved in the polymer solution at a concentration of 3.85 mg/mL. The concentration was determined considering the LD 50 of mice (7.678 mg/kg). The wFIONs were diluted in the polymer solution at a concentration of 100 mM.

Characterization of Thermoresponsive Gelation. The temperature for the sol−gel phase transition of the hydrogel solution was determined at which the storage modulus (G') crosses over the loss modulus (G''). The sol−gel transition temperature is confirmed by using the vial-inverting method. A 4 mL vial was filled with 1 mL of the hydrogel solution, which was kept at various temperatures between 20 and 60 °C at intervals of 5 °C. The phase transition was observed visually by inverting the vial; a gel was defined as the condition in which no flow was observed in the inverted vial. Cryo-TEM (Tecnai G2 F20, Philips) was used to observe the sizes and shapes of the hydrogel and the hydrogel nanocomposite. The time

https://doi.org/10.1021/acsnano.2c10094
ACS Nano 2023, 17, 5435−5447

duration of gelation was measured with a rheometer by monitoring the time-dependent change in the storage modulus (G') and loss modulus (G'') for different temperatures.

In Vivo Measurement of Drug Penetration in the Mouse Brain. The following were administered to mice (C57BL/6, male, 8 weeks) in four groups: (i) coating of the hydrogel nanocomposite with mild hyperthermia; (ii) coating of the hydrogel nanocomposite without mild hyperthermia; (iii) injection of the hydrogel nanocomposite with mild hyperthermia; and (iv) injection of the hydrogel nanocomposite without mild hyperthermia. The hydrogel nanocomposite was dropped on the cerebral cortex surface or injected into the cerebral cortex (using stereotaxic frame; from bregma: AP = +0.5 mm, ML = +2.0 mm, and DV = −4.0 mm). All groups were sutured and treated with hyperthermia. The mice were anesthetized and transcardially perfused with PBS solution (pH 7.4). The brain was extracted and fixed overnight in a 10% neutral buffered formalin solution. The brain tissues were dehydrated with ethanol and then infiltrated and embedded in paraffin. The tissue blocks were serially sectioned by a paraffin microtome (Leica, Germany) into 10 μm thick coronal sections and then collected on slide glasses. The hydrogel nanocomposite was profiled by a confocal laser scanning microscope system (LSM 780 NLO, Carl ZEISS, Germany) with ZEN 3.3 software.

In Vivo Histology Staining and Western Blot Analysis. For the histological analysis, mice were anesthetized and perfused transcardially with a PBS solution (pH 7.4). The brain was extracted and fixed overnight in the 10% neutral buffered formalin solution. The brain tissues were dehydrated with ethanol, then infiltrated and embedded in paraffin. Afterward, paraffin blocks were serially sectioned by a microtome (Leica, Germany) into 4 μm thick coronal sections and then collected on slide glasses. To determine the effect of neuronal changes and reactive gliosis by the injected hydrogel nanocomposite, we treated the tissue slides by the following sequence: deparaffinization, rehydration, and antigen retrieval. Then, they were incubated with the first antibody diluted as 1:500 for neurons (chicken anti-NeuN, Synaptic Systems, Germany), neurofilaments (rabbit anti-NF-L, Abcam, UK), astrocytes (rat anti-GFAP, Invitrogen, USA), and microglia (rabbit anti-Iba1, Abcam, UK) overnight at 4 °C. Next, they were exposed to the second antibody diluted as 1:500 (goat anti-chicken IgY Alexa fluor 488, Invitrogen, USA; goat anti-rabbit IgG Alexa fluor 633, Invitrogen, USA; goat anti-rat IgG Alexa fluor 488, Cell signaling technology, USA). The tissue slides were mounted on a Fluoromount-G (SouthernBiotech, USA) and imaged by confocal microscopy (LSM 780 NLO, Carl ZEISS, Germany).

For the Western blot analysis, the brain was set on the brain-matrix (Ted Pella, USA), and the administration site was transversely cut with a surgical blade. The protein was extracted with an RIPA buffer (R0278, Merck KGaA, Germany) with a protein inhibitor (ab65621, Abcam, UK). After centrifugation, the protein level in the supernatants was determined using a Micro BCA Protein Assay Kit with bovine serum albumin as the standard (Pierce, USA). Aliquots containing a total protein amount of 20 μg were boiled in a buffer containing 150 mM Tris (pH 6.8), 3 mM DTT, 6% SDS, 0.3% bromophenol blue, and 30% glycerol. The aliquots were then loaded onto a 15% acrylamide gel. After electrophoresis, the gels were transferred to the PVDF membrane (Immobilon-P PVDF membrane, Millipore). To reduce background staining, the membranes were incubated with 5% bovine serum albumin in the Tris-buffered saline solution for 1 h, followed by incubation with the first antibody (rabbit anti-GAPDH, 1:2000, Abcam, UK; rabbit anti-NeuN, 2 μg/mL, Abcam, UK; rabbit anti-NF-L, 1:1000, Abcam, UK; rabbit anti-GFAP, 1:5000, Abcam, UK; goat anti-Iba1, 1 μg/mL, Novus biologicals, USA), the second antibody (goat anti-rabbit IgG-HRP, 1:5000, Abcam, UK; donkey anti-goat IgG-HRP, 1:5000, Merck KGaA), and an ECL kit (Amersham, UK). The Western blot analysis was repeated three times. The results were scanned by a Bioimaging system (Amersham imager 600, Amersham) and quantified by ImageJ software.

In Vivo MR Imaging for the Biodegradability Evaluation. To evaluate the biodegradability of the nanocomposite in the brain, we conducted MR imaging in the subcutaneous and intratumoral regions of the mouse (MRS*DRYMAG 3-T MR scanner, MR Solutions, Guildford, UK). The hydrogel nanocomposite and tissues were measured by a fast spin−echo (FSE) sequence to obtain T2-weighted images. The measurement parameters for brain MR images were as follows: repetition time = 5000 ms, effective echo time = 68 ms, echo train = 8, echo spacing = 17 ms, number of data for average = 3, field-of-view = 30 × 30 mm, matrix = 240 × 256, slice thickness = 0.8 mm, flip angle = 90°, total slices = 12, and acquisition duration = 461 s. In the obtained brain MR images, the region of the hydrogel nanocomposite could be distinguished. A thresholding method was used for image segmentation and processing. ImageJ software was used to analyze the MR images on day 1 to choose appropriate hydrogel nanocomposite regions on the basis of the minimum threshold. Then, the mean values of signal intensities on the regions were acquired from images at various time points. We measured the mean value of the MR signal intensities over the cortex area and calculated the ratio of the MR signal intensities between the hydrogel nanocomposite region and the cortex area. The signal intensity ratio was normalized to the ratio obtained from the MR image on day 1.

In Vivo Tumor Treatment Using the Mouse Tumor Resection Model. To prepare the orthotopic mouse brain GBM model, about 2 × 10^5 U-87 MG-Luc2 cells were injected into the cerebral cortex (using stereotaxic frame; from bregma: AP = +0.5 mm, ML = +2.0 mm, and DV = −2.0 mm). The luminescence intensity from the U-87 MG-Luc2 cells was imaged using an IVIS (IVIS Lumina II, Caliper Life Sciences) and quantified using Living Image software (PerkinElmer). The time point of the resection surgery was determined by considering the morphology and volume of the implanted tumors measured by using MR and IVIS imaging (typically 2 weeks after the GBM cell injection). The implanted tumor grew over 1 mm in width, depth, and height, respectively, according to MR imaging and also showed a consistent increase in bioluminescence intensity in IVIS imaging for 2 weeks. The resection surgery consisted of tumor removal with a surgical drill, suction of the resected tumor, and hemostasis in order. Then, the mice treated with resection surgery were randomly assigned to five groups: (i) resection and injection of PBS (control group); (ii) resection and injection of the hydrogel nanocomposite without drug but with mild hyperthermia (heating group); (iii) resection and coating of the hydrogel nanocomposite without mild hyperthermia (coating group); (iv) resection and injection of the hydrogel nanocomposite without mild hyperthermia (injection group); (v) resection and injection of the hydrogel nanocomposite with mild hyperthermia (treatment group).

The experimental procedures for the control, heating, coating, injection, and treatment groups are as follows. PBS (control group) or the hydrogel nanocomposite (heating, injection, and treatment groups) was injected at four locations 0.3 mm from the center of the resected tumor. Subsequently, the rest of the PBS (control group) or the hydrogel nanocomposite (heating, injection, and treatment groups) was dropped onto the injected postoperative surgical cavity. For the coating group, the hydrogel nanocomposite is applied on the surface of the resected GBM site. Then, the bioglue (EVICEL, Ethicon, USA) was dropped on the surface for heating, coating, injection, and nanocomposite groups. Next, all groups were sutured and treated with 5% glucose as postoperative care. The heating and treatment groups were treated with mild hyperthermia. The mice were anesthetized, and mild hyperthermia was applied following the same condition as the *in vitro* experimental method. This treatment was conducted once every 2 days for 2 weeks.

Statistical Analysis. The Mann−Whitney U-test was used to compare the quantification results of immunohistochemistry and Western blot analysis. The tumor volume for all mice in each group was measured and compared using the one-way ANOVA test with the Scheffe multiple-comparisons test. The log-rank test was used to compare the survival plots of each group.

Ethical Approval. This study was approved by the Institutional Animal Care and Use Committee (IACUC; No. SNU-210630) and

https://doi.org/10.1021/acsnano.2c10094
ACS Nano 2023, 17, 5435−5447

performed according to the IACUC guidelines and with the National Institute of Health Guide for the Care and Use of Laboratory Animals. Researchers who carried out the surgery, managed the animal, and measured the tumor volume were blinded to one another.

Other Methods. Other methods, such as the detailed synthesis and characterization of the materials, *in vitro* cellular experiment methods, and *in vivo* histological analysis, are included in the Supporting Information.

ASSOCIATED CONTENT

Data Availability Statement

The data that support the findings of this study are available from the corresponding author upon reasonable request.

Supporting Information

The Supporting Information is available free of charge at https://pubs.acs.org/doi/10.1021/acsnano.2c10094.

Additional experimental details, including synthesis of wFIONs, synthesis of the drug-loaded micelle, confocal microscopy observation of the hydrogel nanocomposite, *in vitro* wireless mild hyperthermia, measurement of the hydrogel mesh size, *in vitro* DOX/wFIONs release profile from the hydrogel nanocomposite, characterization of the drug-loaded micelle, and *in vitro* cellular study; Figures S1−S11 of characterization of the thermoresponsive hydrogel, characterization of wFIONs and their hyperthermic effect, synthesis and characterization of the DOX-loaded micelles, incorporating another type of drug into micelles, uptake of the DOX-loaded micelle by U-87 MG cells, biodegradability of the hydrogel nanocomposite, biodegradability of the hydrogel nanocomposite in intramuscular and subcutaneous regions, stability of the hydrogel nanocomposite, Western blot analysis of the brain tissue injected with the hydrogel nanocomposite, preparation of the GBM resection model in the mouse brain, relative change of bioluminescence intensity 4 weeks after the treatment, and *in vivo* histology (PDF)

AUTHOR INFORMATION

Corresponding Authors

Taeghwan Hyeon − *Center for Nanoparticle Research, Institute for Basic Science (IBS), Seoul 08826, Republic of Korea; School of Chemical and Biological Engineering, Institute of Chemical Processes, Seoul National University, Seoul 08826, Republic of Korea;* orcid.org/0000-0001-5959-6257; Email: thyeon@snu.ac.kr

Dae-Hyeong Kim − *Center for Nanoparticle Research, Institute for Basic Science (IBS), Seoul 08826, Republic of Korea; School of Chemical and Biological Engineering, Institute of Chemical Processes, Seoul National University, Seoul 08826, Republic of Korea; Department of Materials Science and Engineering, Seoul National University, Seoul 08826, Republic of Korea;* orcid.org/0000-0002-4722-1893; Email: dkim98@snu.ac.kr

Seung Hong Choi − *Center for Nanoparticle Research, Institute for Basic Science (IBS), Seoul 08826, Republic of Korea; Department of Radiology, Seoul National University College of Medicine, Seoul 03080, Republic of Korea;* Email: verocay1@snu.ac.kr

Authors

Taegyu Kang − *Center for Nanoparticle Research, Institute for Basic Science (IBS), Seoul 08826, Republic of Korea; School of Chemical and Biological Engineering, Institute of Chemical Processes, Seoul National University, Seoul 08826, Republic of Korea;* orcid.org/0000-0001-9032-7362

Gi Doo Cha − *Center for Nanoparticle Research, Institute for Basic Science (IBS), Seoul 08826, Republic of Korea; School of Chemical and Biological Engineering, Institute of Chemical Processes, Seoul National University, Seoul 08826, Republic of Korea; Department of Radiology, Seoul National University College of Medicine, Seoul 03080, Republic of Korea;* orcid.org/0000-0002-4771-3396

Ok Kyu Park − *Center for Nanoparticle Research, Institute for Basic Science (IBS), Seoul 08826, Republic of Korea; Department of Radiology, Seoul National University College of Medicine, Seoul 03080, Republic of Korea*

Hye Rim Cho − *Center for Nanoparticle Research, Institute for Basic Science (IBS), Seoul 08826, Republic of Korea; Department of Radiology, Seoul National University College of Medicine, Seoul 03080, Republic of Korea*

Minjeong Kim − *Center for Nanoparticle Research, Institute for Basic Science (IBS), Seoul 08826, Republic of Korea; School of Chemical and Biological Engineering, Institute of Chemical Processes, Seoul National University, Seoul 08826, Republic of Korea*

Jongha Lee − *Center for Nanoparticle Research, Institute for Basic Science (IBS), Seoul 08826, Republic of Korea; School of Chemical and Biological Engineering, Institute of Chemical Processes, Seoul National University, Seoul 08826, Republic of Korea*

Dokyoon Kim − *Center for Nanoparticle Research, Institute for Basic Science (IBS), Seoul 08826, Republic of Korea; Department of Bionano Engineering, Hanyang University, Ansan 15588, Republic of Korea*

Bowon Lee − *Center for Nanoparticle Research, Institute for Basic Science (IBS), Seoul 08826, Republic of Korea; School of Chemical and Biological Engineering, Institute of Chemical Processes, Seoul National University, Seoul 08826, Republic of Korea*

Jinyoung Chu − *Center for Nanoparticle Research, Institute for Basic Science (IBS), Seoul 08826, Republic of Korea; School of Chemical and Biological Engineering, Institute of Chemical Processes, Seoul National University, Seoul 08826, Republic of Korea*

Sagang Koo − *Center for Nanoparticle Research, Institute for Basic Science (IBS), Seoul 08826, Republic of Korea; School of Chemical and Biological Engineering, Institute of Chemical Processes, Seoul National University, Seoul 08826, Republic of Korea;* orcid.org/0000-0001-8154-7881

Complete contact information is available at: https://pubs.acs.org/10.1021/acsnano.2c10094

Author Contributions

†T. Kang, G. D. Cha, and O. K. Park contributed equally to this work.

Notes

The authors declare no competing financial interest.

ACKNOWLEDGMENTS

This work was supported by Institute for Basic Science (IBS-R006-D1 and IBS-R006-A1), Creative-Pioneering Researchers Program through Seoul National University (SNU), and the SNUH Research Fund (No. 0320212010 (2021-2556)). We

acknowledge the help from Anton Paar Korea to measure the gelation.

REFERENCES

(1) Weller, M.; van den Bent, M.; Preusser, M.; Le Rhun, E.; Tonn, J. C.; Minniti, G.; Bendszus, M.; Balana, C.; Chinot, O.; Dirven, L.; French, P.; Hegi, M. E.; Jakola, A. S.; Platten, M.; Roth, P.; Ruda, R.; Short, S.; Smits, M.; Taphoorn, M. J. B.; von Deimling, A.; et al. EANO Guidelines on the Diagnosis and Treatment of Diffuse Gliomas of Adulthood. *Nat. Rev. Clin. Oncol.* **2021**, *18*, 170−186.

(2) Yang, I.; Aghi, M. K. New Advances That Enable Identification of Glioblastoma Recurrence. *Nat. Rev. Clin. Oncol.* **2009**, *6*, 648−657.

(3) Stupp, R.; Mason, W. P.; van den Bent, M. J.; Weller, M.; Fisher, B.; Taphoorn, M. J. B.; Belanger, K.; Brandes, A. A.; Marosi, C.; Bogdahn, U.; Curschmann, J.; Janzer, R. C.; Ludwin, S. K.; Gorlia, T.; Allgeier, A.; Lacombe, D.; Cairncross, J. G.; Eisenhauer, E.; Mirimanoff, R. O.; Van Den Weyngaert, D.; et al. Radiotherapy Plus Concomitant and Adjuvant Temozolomide for Glioblastoma. *New Engl. J. Med.* **2005**, *352*, 987−996.

(4) Cha, G. D.; Kang, T.; Baik, S.; Kim, D.; Choi, S. H.; Hyeon, T.; Kim, D. H. Advances in Drug Delivery Technology for the Treatment of Glioblastoma Multiforme. *J. Controlled Release* **2020**, *328*, 350−367.

(5) Arvanitis, C. D.; Ferraro, G. B.; Jain, R. K. The Blood-Brain Barrier and Blood-Tumour Barrier in Brain Tumours and Metastases. *Nat. Rev. Cancer* **2020**, *20*, 26−41.

(6) Klein, M.; Heimans, J. J.; Aaronson, N. K.; van der Ploeg, H. M.; Grit, J.; Muller, M.; Postma, T. J.; Mooij, J. J.; Boerman, R. H.; Beute, G. N.; Ossenkoppele, G. J.; van Imhoff, G. W.; Dekker, A. W.; Jolles, J.; Slotman, B. J.; Struikmans, H.; Taphoorn, M. J. B. Effect of Radiotherapy and Other Treatment-related Factors on Mid-Term to Long-Term Cognitive Sequelae in Low-Grade Gliomas: a Comparative Study. *Lancet* **2002**, *360*, 1361−1368.

(7) Lober-Handwerker, R.; Doring, K.; Bock, C.; Rohde, V.; Malinova, V. Defining the Impact of Adjuvant Treatment on the Prognosis of Patients with Inoperable Glioblastoma Undergoing Biopsy Only: Does the Survival Benefit Outweigh the Treatment Effort? *Neurosurg. Rev.* **2022**, *45*, 2339−2347.

(8) Zou, Y.; Sun, X. H.; Yang, Q. S.; Zheng, M.; Shimoni, O.; Ruan, W. M.; Wang, Y. B.; Zhang, D. Y.; Yin, J. L.; Huang, X. G.; Tao, W.; Park, J. B.; Liang, X. J.; Leong, K. W.; Shi, B. Y. Blood-brain Barrier-Penetrating Single CRISPR-Cas9 Nanocapsules for Effective and Safe Glioblastoma Gene Therapy. *Sci. Adv.* **2022**, *8*, eabm8011.

(9) Kievit, F. M.; Veiseh, O.; Fang, C.; Bhattarai, N.; Lee, D.; Ellenbogen, R. G.; Zhang, M. Q. Chlorotoxin Labeled Magnetic Nanovectors for Targeted Gene Delivery to Glioma. *ACS Nano* **2010**, *4*, 4587−4594.

(10) Ni, D. L.; Zhang, J. W.; Bu, W. B.; Xing, H. Y.; Han, F.; Xiao, Q. F.; Yao, Z. W.; Chen, F.; He, Q. J.; Liu, J. N.; Zhang, S. J.; Fan, W. P.; Zhou, L. P.; Peng, W. J.; Shi, J. L. Dual-Targeting Upconversion Nanoprobes across the Blood-Brain Barrier for Magnetic Resonance/Fluorescence Imaging of Intracranial Glioblastoma. *ACS Nano* **2014**, *8*, 1231−1242.

(11) Shen, Z. Y.; Liu, T.; Li, Y.; Lau, J.; Yang, Z.; Fan, W. P.; Zhou, Z. J.; Shi, C. R.; Ke, C. M.; Bregadze, V. I.; Mandal, S. K.; Liu, Y. J.; Li, Z. H.; Xue, T.; Zhu, G. Z.; Munasinghe, J.; Niu, G.; Wu, A. G.; Chen, X. Y. Fenton-Reaction-Acceleratable Magnetic Nanoparticles for Ferroptosis Therapy of Orthotopic Brain Tumors. *ACS Nano* **2018**, *12*, 11355−11365.

(12) Jensen, S. A.; Day, E. S.; Ko, C. H.; Hurley, L. A.; Luciano, J. P.; Kouri, F. M.; Merkel, T. J.; Luthi, A. J.; Patel, P. C.; Cutler, J. I.; Daniel, W. L.; Scott, A. W.; Rotz, M. W.; Meade, T. J.; Giljohann, D. A.; Mirkin, C. A.; Stegh, A. H. Spherical Nucleic Acid Nanoparticle Conjugates as an RNAi-Based Therapy for Glioblastoma. *Sci. Transl. Med.* **2013**, *5*, 209ra152.

(13) van Solinge, T. S.; Nieland, L.; Chiocca, E. A.; Broekman, M. L. D. Advances in Local Therapy for Glioblastoma - Taking the Fight to the Tumour. *Nat. Rev. Neurol.* **2022**, *18*, 221−236.

(14) Mathios, D.; Kim, J. E.; Mangraviti, A.; Phallen, J.; Park, C. K.; Jackson, C. M.; Garzon-Muvdi, T.; Kim, E.; Theodros, D.; Polanczyk, M.; Martin, A. M.; Suk, I.; Ye, X. B.; Tyler, B.; Bettegowda, C.; Brem, H.; Pardoll, D. M.; Lim, M. Anti-PD-1 Antitumor Immunity Is Enhanced by Local and Abrogated by Systemic Chemotherapy in GBM. *Sci. Transl. Med.* **2016**, *8*, 370ra180.

(15) Voth, B. L.; Pelargos, P. E.; Barnette, N. E.; Bhatt, N. S.; Chen, C. H. J.; Lagman, C.; Chung, L. K.; Nguyen, T.; Sheppard, J. P.; Romiyo, P.; Mareninov, S.; Kickhoefer, V. A.; Yong, W. H.; Rome, L. H.; Yang, I. Intratumor Injection of CCL21-coupled Vault Nanoparticles Is Associated with Reduction in Tumor Volume in an in Vivo Model of Glioma. *J. Neuro-Oncol.* **2020**, *147*, 599−605.

(16) Wang, Y. H.; Jiang, Y. H.; Wei, D. S.; Singh, P.; Yu, Y. J.; Lee, T.; Zhang, L. P.; Mandl, H. K.; Piotrowski-Daspit, A. S.; Chen, X. Y.; Li, F.; Li, X.; Cheng, Y. Y.; Josowitz, A.; Yang, F.; Zhao, Y.; Wang, F. Y.; Zhao, Z. W.; Huttner, A.; Bindra, R. S.; et al. Nanoparticle-Mediated Convection-Enhanced Delivery of a DNA Intercalator to Gliomas Circumvents Temozolomide Resistance. *Nat. Biomed. Eng.* **2021**, *5*, 1048−1058.

(17) Stephen, Z. R.; Kievit, F. M.; Veiseh, O.; Chiarelli, P. A.; Fang, C.; Wang, K.; Hatzinger, S. J.; Ellenbogen, R. G.; Silber, J. R.; Zhang, M. Q. Redox-Responsive Magnetic Nanoparticle for Targeted Convection-Enhanced Delivery of O-6-Benzylguanine to Brain Tumors. *ACS Nano* **2014**, *8*, 10383−10395.

(18) Seo, Y. E.; Suh, H. W.; Bahal, R.; Josowitz, A.; Zhang, J. W.; Song, E.; Cui, J. J.; Noorbakhsh, S.; Jackson, C.; Bu, T.; Piotrowski-Daspit, A.; Bindra, R.; Saltzman, W. M. Nanoparticle-Mediated Intratumoral Inhibition of miR-21 for Improved Survival in Glioblastoma. *Biomaterials* **2019**, *201*, 87−98.

(19) Lesniak, M. S.; Brem, H. Targeted Therapy for Brain Tumours. *Nat. Rev. Drug. Discovery* **2004**, *3*, 499−508.

(20) Acarón Ledesma, H.; Li, X.; Carvalho-de-Souza, J. L.; Wei, W.; Bezanilla, F.; Tian, B. an Atlas of Nano-Enabled Neural Interfaces. *Nat. Nanotechnol.* **2019**, *14*, 645−657.

(21) Jain, A.; Betancur, M.; Patel, G. D.; Valmikinathan, C. M.; Mukhatyar, V. J.; Vakharia, A.; Pai, S. B.; Brahma, B.; MacDonald, T. J.; Bellamkonda, R. V. Guiding Intracortical Brain Tumour Cells to an Extracortical Cytotoxic Hydrogel Using Aligned Polymeric Nanofibres. *Nat. Mater.* **2014**, *13*, 308−316.

(22) Bastiancich, C.; Vanvarenberg, K.; Ucakar, B.; Pitorre, M.; Bastiat, G.; Lagarce, F.; Preat, V.; Danhier, F. Lauroyl-Gemcitabine-Loaded Lipid Nanocapsule Hydrogel for the Treatment of Glioblastoma. *J. Controlled Release* **2016**, *225*, 283−293.

(23) Zhang, J.; Chen, C.; Li, A. N.; Jing, W. Q.; Sun, P.; Huang, X. Y.; Liu, Y. C.; Zhang, S. C.; Du, W.; Zhang, R.; Liu, Y.; Gong, A. H.; Wu, J. B.; Jiang, X. Y. Immunostimulant Hydrogel for the Inhibition of Malignant Glioma Relapse Post-Resection. *Nat. Nanotechnol.* **2021**, *16*, 538−548.

(24) Birocchi, F.; Cusimano, M.; Rossari, F.; Beretta, S.; Rancoita, P. M. V.; Ranghetti, A.; Colombo, S.; Costa, B.; Angel, P.; Sanvito, F.; Callea, M.; Norata, R.; Chaabane, L.; Canu, T.; Spinelli, A.; Genua, M.; Ostuni, R.; Merelli, I.; Coltella, N.; Naldini, L. Targeted Inducible Delivery of Immunoactivating Cytokines Reprograms Glioblastoma Microenvironment and Inhibits Growth in Mouse Models. *Sci. Transl. Med.* **2022**, *14*, eabl4106.

(25) Lee, Y.; Kang, T.; Cho, H. R.; Lee, G. J.; Park, O. K.; Kim, S.; Lee, B.; Kim, H. M.; Cha, G. D.; Shin, Y.; Lee, W.; Kim, M.; Kim, H.; Song, Y. M.; Choi, S. H.; Hyeon, T.; Kim, D.-H. Localized Delivery of Theranostic Nanoparticles and High-Energy Photons Using Microneedles-on-Bioelectronics. *Adv. Mater.* **2021**, *33*, 2100425.

(26) Di Mascolo, D.; Palange, A. L.; Primavera, R.; Macchi, F.; Catelani, T.; Piccardi, F.; Spano, R.; Ferreira, M.; Marotta, R.; Armirotti, A.; Gallotti, A. L.; Galli, R.; Wilson, C.; Grant, G. A.; Decuzzi, P. Conformable Hierarchically Engineered Polymeric Micromeshes Enabling Combinatorial Therapies in Brain Tumours. *Nat. Nanotechnol.* **2021**, *16*, 820−829.

(27) Lee, J.; Cho, H. R.; Cha, G. D.; Seo, H.; Lee, S.; Park, C.-K.; Kim, J. W.; Qiao, S.; Wang, L.; Kang, D.; Kang, T.; Kim, T. I. J.; Lee, H.; Lee, W.; Kim, S.; Lee, S.-T.; Lu, N.; Hyeon, T.; Choi, S. H.; Kim,

https://doi.org/10.1021/acsnano.2c10094
ACS Nano 2023, 17, 5435−5447

D.-H. Flexible, sticky, and Biodegradable Wireless Device for Drug Delivery to Brain Tumors. *Nat. Commun.* **2019**, *10*, 5205−5213.
(28) Jeong, B.; Bae, Y. H.; Lee, D. S.; Kim, S. W. Biodegradable Block Copolymers as Injectable Drug-Delivery Systems. *Nature* **1997**, *388*, 860−862.
(29) Yoo, H. S.; Lee, E. A.; Park, T. G. Doxorubicin-Conjugated Biodegradable Polymeric Micelles Having Acid-Cleavable Linkages. *J. Controlled Release* **2002**, *82*, 17−27.
(30) Lee, N.; Choi, Y.; Lee, Y.; Park, M.; Moon, W. K.; Choi, S. H.; Hyeon, T. Water-Dispersible Ferrimagnetic Iron Oxide Nanocubes with Extremely High r(2) Relaxivity for Highly Sensitive in Vivo MRI of Tumors. *Nano Lett.* **2012**, *12*, 3127−3131.
(31) Liu, S. H.; Guo, Y. B.; Huang, R. Q.; Li, J. F.; Huang, S. X.; Kuang, Y. Y.; Han, L.; Jiang, C. Gene and Doxorubicin Co-Delivery System for Targeting Therapy of Glioma. *Biomaterials* **2012**, *33*, 4907−4916.
(32) Bi, Y. K.; Liu, L. S.; Lu, Y. F.; Sun, T.; Shen, C.; Chen, X. L.; Chen, Q. J.; An, S.; He, X.; Ruan, C. H.; Wu, Y. H.; Zhang, Y. J.; Guo, Q.; Zheng, Z. X.; Liu, Y. H.; Lou, M. Q.; Zhao, S. G.; Jiang, C. T7 Peptide-Functionalized PEG-PLGA Micelles Loaded with Carmustine for Targeting Therapy of Glioma. *ACS Appl. Mater. Interfaces* **2016**, *8*, 27465−27473.
(33) Cui, Y.; Zhang, M.; Zeng, F.; Jin, H. Y.; Xu, Q.; Huang, Y. Z. Dual-Targeting Magnetic PLGA Nanoparticles for Codelivery of Paclitaxel and Curcumin for Brain Tumor Therapy. *ACS Appl. Mater. Interfaces* **2016**, *8*, 32159−32169.
(34) Cagel, M.; Grotz, E.; Bernabeu, E.; Moretton, M. A.; Chiappetta, D. A. Doxorubicin: Nanotechnological Overviews from Bench to Bedside. *Drug Discovery Today* **2017**, *22*, 270−281.
(35) Annovazzi, L.; Caldera, V.; Mellai, M.; Riganti, C.; Battaglia, L.; Chirio, D.; Melcarne, A.; Schiffer, D. The DNA Damage/Repair Cascade in Glioblastoma Cell Lines after Chemotherapeutic Agent Treatment. *Int. J. Oncol.* **2015**, *46*, 2299−2308.
(36) Voulgaris, S.; Partheni, M.; Karamouzis, M.; Dimopoulos, P.; Papadakis, N.; Kalofonos, H. P. Intratumoral Doxorubicin in Patients with Malignant Brain Gliomas. *Am. J. Clin. Oncol.* **2002**, *25*, 60−64.
(37) Lee, N.; Yoo, D.; Ling, D.; Cho, M. H.; Hyeon, T.; Cheon, J. Iron Oxide Based Nanoparticles for Multimodal Imaging and Magnetoresponsive Therapy. *Chem. Rev.* **2015**, *115*, 10637−10689.
(38) Weldon, C.; Tian, B. Z.; Kohane, D. S. Nanotechnology for Surgeons. *Wiley Interdiscip. Rev. Nanomed. Nanobiotechnol.* **2011**, *3*, 223−228.
(39) Wolf, K. J.; Chen, J.; Coombes, J. D.; Aghi, M. K.; Kumar, S. Dissecting and Rebuilding the Glioblastoma Microenvironment with Engineered Materials. *Nat. Rev. Mater.* **2019**, *4*, 651−668.
(40) Hynynen, K. Hyperthermia-Induced Drug Delivery in Humans. *Nat. Biomed. Eng.* **2018**, *2*, 637−639.
(41) Li, J. Y.; Mooney, D. J. Designing Hydrogels for Controlled Drug Delivery. *Nat. Rev. Mater.* **2016**, *1*, 16071.
(42) Bourrinet, P.; Bengele, H. H.; Bonnemain, B.; Dencausse, A.; Idee, J. M.; Jacobs, P. M.; Lewis, J. M. Preclinical Safety and Pharmacokinetic Profile of Ferumoxtran-10, an Ultrasmall Superparamagnetic Iron Oxide Magnetic Resonance Contrast Agent. *Invest. Radiol.* **2006**, *41*, 313−324.
(43) Zhou, T.; Hong, G.; Fu, T. M.; Yang, X.; Schuhmann, T. G.; Viveros, R. D.; Lieber, C. M. Syringe-Injectable Mesh Electronics Integrate Seamlessly with Minimal Chronic Immune Response in the Brain. *Proc. Natl. Acad. Sci. U.S.A.* **2017**, *114*, 5894−5899.
(44) Jenkins, E. P. W.; Finch, A.; Gerigk, M.; Triantis, I. F.; Watts, C.; Malliaras, G. G. Electrotherapies for Glioblastoma. *Adv. Sci.* **2021**, *8*, 2100978.
(45) Aldape, K.; Brindle, K. M.; Chesler, L.; Chopra, R.; Gajjar, A.; Gilbert, M. R.; Gottardo, N.; Gutmann, D. H.; Hargrave, D.; Holland, E. C.; Jones, D. T. W.; Joyce, J. A.; Kearns, P.; Kieran, M. W.; Mellinghoff, I. K.; Merchant, M.; Pfister, S. M.; Pollard, S. M.; Ramaswamy, V.; Rich, J. N.; et al. Challenges to Curing Primary Brain Tumours. *Nat. Rev. Clin. Oncol.* **2019**, *16*, 509−520.
(46) Shi, K.; Wang, Y. L.; Qu, Y.; Liao, J. F.; Chu, B. Y.; Zhang, H. P.; Luo, F.; Qian, Z. Y. Synthesis, Characterization, and Application of Reversible PDLLA-PEG-PDLLA Copolymer Thermogels in Vitro and in Vivo. *Sci. Rep.* **2016**, *6*, 19077.

https://doi.org/10.1021/acsnano.2c10094
ACS Nano 2023, 17, 5435−5447